International Journal of Thermophysics, Vol. 22, No. 2, 2001

Specific Heat and Thermal Transport Measurements of Reactive Metallic Alloys by Noncontact Calorimetry in Reduced Gravity[1]

R. K. Wunderlich,[2, 3] Ch. Ettl,[2] and H.-J. Fecht[2]

Experimental concepts, application, and recent results of noncontact calorimetry inculding ac-specific heat and thermal transport property measurement of reactive metallic specimens are described. The method is based on induction heating in an electromagnetic levitation device. Experiments have been performed in reduced gravity onboard Spacelab. A heat flow model is discussed regarding conditions for precise specific heat determination from the temperature response to modulated heating power input as well as determination of thermal transport properties from the transient temperature response. Modulation techniques were developed for application in the metastable regime of the undercooled melt, where processing time is a critical issue. Results to be discussed include the total hemispherical emissivity of a bulk metallic glass-forming alloy revealing effects of surface segregation, thermal conductivity measurements, and application of ac calorimetry in the two-phase region.

KEY WORDS: containerless processing; liquid metals; modulation calorimetry; thermophysical properties..

1. INTRODUCTION

Noncontact ac calorimetry based on induction heating in an electromagnetic levitation device has been developed for the investigation of the thermodynamic properties of reactive metallic specimens in the stable and undercooled liquid phase. The method was proposed by Fecht and

[1] Paper presented at the Fourteenth Symposium on Thermophysical Properties, June 25–30, 2000, Boulder, Colorado, U.S.A.

[2] Abteilung Werkstoffe der Elektrotechnik, Universität Ulm, Albert-Einstein-Allee 47, D-89081 Ulm, Germany.

[3] To whom correspondence should be addressed. E-mail: rainer.wunderlich@e-technik.uni-ulm.de

0195-928X/01/0300-0579$19.50/0

Johnson [1] with the basic heat flow model based on the early work of Sullivan and Seidel [2]. For metallic specimens, modulation calorimetry by direct volume heating has been described in detail by Kraftmakher [3].

In this article we describe recent developments of noncontact ac calorimetry and results obtained in two Spacelab missions. The work originated out of a program for the investigation of the thermophysical properties of Zr-based metallic glass forming alloys in the liquid phase. Microgravity (μg) conditions were motivated by the requirement of high undercooling and quiescent specimen conditions which cannot be obtained under 1-*g* conditions due to the excessive heating effects associated with 1-*g* levitation and the relatively low liquidus or eutectic temperature of the specimens to be investigated. In addition, μg conditions provide for a nearly spherical specimen shape, facilitating considerably the determination of electromagnetic power consumption and radiative heat loss.

In Section 2, the experimental concept, with emphasis on the conditions of isothermal modulation, particular modulation techniques for application in the undercooled liquid, and evaluation of relaxation times, is described. In Section 3, some typical experimental results showing the applicability of the method to the measurement of thermal transport properties as well as in the two-phase region are described.

2. EXPERIMENTAL CONCEPT

For application of noncontact electromagnetic ac calorimetry, an electrically conducting spherical specimen is positioned by a radiofrequency (rf) quadrupole positioning field (positioner) and heated by an rf dipole field with the resulting temperature measured by a pyrometer. Temperature control is performed by variation of the control voltage of the heater generator. The frequency of the positioner and heater are different allowing separation of the total rf power input as $P_{\text{in}} = P_{\text{H}} + P_{\text{P}}$, with P_{H} and P_{P} the power induced by the heater and positioner, respectively. This separation is important, allowing one to perform quantitative ac calorimetry by modulating the heater field in the presence of positioning fields. Quantification is based on determination of the modulated component(s) of induction power input, P_ω, and by choosing a modulation frequency allowing one to neglect the effects of the finite thermal conductivity and radiative heat loss resulting in a uniform amplitude of temperature modulation (isothermal modulation). P_ω, as well as the specimen resistivity, ρ, can be obtained from inductive resistivity measurement [4] after proper calibration of the electromagnetic coupling efficiency [5, 6].

The method was implemented in the containerless electromagnetic processing device TEMPUS described in detail elsewhere [7]. Relevant to

the work presented here, TEMPUS provides for high-resolution pyrometric temperature [8], thermal expansion [9], and current and voltage measurement of the rf heater and positioner oscillating circuit.

2.1. Heat Flow Model

To investigate the conditions for quantitative noncontact ac calorimetry regarding isothermal modulation, and to obtain corrections when these conditions cannot be met as well as for devising methods for the measurement of thermal relaxation times, a simple heat flow model is constructed. The heat flow model is obtained by considering the spatial heating power distribution in a spherical specimen of radius R, exposed to an rf dipole field [10]. The field axis defines the polar position where temperature measurement is performed. Heating power input has azimuthal symmetry and tends to zero for a polar angle smaller than 20°. Heating power is a maximum in the equatorial plane with a skin depth of the rf heater field close to 1 mm. As such, the specimen is divided in a directly heated volume fraction, g_H, and a conductively heated volume fraction, $1-g_H$, with corresponding surface fractions of s_H and $1-s_H$, respectively.

For specimens typical for this investigation, i.e., liquid transition metal alloys with $R=4$ mm and resistivity $\rho=140\ \mu\Omega\cdot\text{cm}$, $g_H\approx 0.4$. The amplitude of temperature modulation at a frequency ω measured at the polar position, $\Delta T_{S\omega}$, exhibits the typical ω dependence of a conductively heated reservoir with a decrease in $\Delta T_{S\omega}$ as a function of ω, while the corresponding $\Delta T_{H\omega}$ measured at the equatorial position is characterized by an increase. Writing the total inductive power input as $P_{in}(t)=P_o+\Delta P(t)$, the following system of equations is obtained for a specimen with heat capacity C_P:

$$\begin{aligned} g_H C_P\,\Delta\dot{T}_H(t) &= \Delta P(t) - kc[\Delta T_H(t)-\Delta T_S(t)] - krh\,\Delta T_H(t) \\ (1-g_H)\,C_P\,\Delta\dot{T}_S(t) &= kc[\Delta T_H(t)-\Delta T_S(t)] - krs\,\Delta T_S(t) \end{aligned} \tag{1}$$

$\Delta T_H(t)$ and $\Delta T_S(t)$ are the deviations from the equilibrium temperatures, T_{Ho} and T_{So}, of the inductively and conductively heated volume fractions, respectively, on application of the power modulation. $\Delta P(t)$ is chosen such that $\Delta T_{H,S}(t)/T_{Ho,So}\ll 1$. kc describes the rate of conductive heat transfer in $\text{W}\cdot\text{K}^{-1}$. krh and krs represent the rate of radiative heat loss of the directly and conductively heated volume fraction.

The following approximations have been made: (i) linearization of the radiative boundary condition justified by the small change in average temperature due to modulation, and (ii) absence of stationary temperature gradients, i.e., $T_{Ho}\approx T_{So}\approx T_o$. The latter approximation is equivalent to

$\mathrm{Bi} \leqslant 0.01$ with the Biot number, Bi, specifying the ratio of internal heat transport to external heat loss. $\mathrm{Bi} \leqslant 0.01$ is readily obtained for metallic specimens. With these approximations,

$$kr = 4A\sigma\varepsilon T_{\mathrm{o}}^3 \qquad \text{and} \qquad krh = krs_{\mathrm{H}}, \qquad krs = kr(1 - s_{\mathrm{H}}) \tag{2}$$

A, σ, and ε are the surface area, the Stefan–Bolzmann constant, and the total hemispherical emissivity, respectively. kc can be approximated by

$$kc = 4\pi(R - \gamma\delta)\,\kappa \tag{3}$$

with κ the thermal conductivity, and γ a geometry factor taking into account the dependence of the heating power input on the polar angle. $\gamma \approx 0.65$, is obtained from an analytical calculation of the spatial distribution of the heating power input [10].

2.2. Temperature Response

Depending on the particular $\Delta P(t)$, the temperature response to heating power modulation is characterized by an increase in average temperature, ΔT_{av}, a transient for each frequency component with amplitude ΔT_{ω}, and stationary modulation terms with amplitudes ΔT_{ω} as shown in Eq. (4). Calorimetric measurement parameters are ΔT_{Hav}, ΔT_{Sav}, $\Delta T_{\mathrm{H}\omega,\,\mathrm{S}\omega}$, the phase shifts between $\Delta T_{\mathrm{H,\,S}}(t)$ and $\Delta P_{\omega}(t)$, the current and voltage of the rf heater boscillating circuit, and the time constants of the transient temperature response. The latter are given by the eigenvalues, λ_1 and λ_2, of the coefficient matrix of Eq. (1). For $\mathrm{Bi} \leqslant 0.01$, $|\lambda_1| \ll |\lambda_2|$ and λ_1 dominates the transient response after a short time. For $\Delta P(t) = \Delta P_{\mathrm{av}} + P_{\omega}\sin(\omega t + \phi_0)$, the temperature response at the polar position is

$$\begin{aligned}\Delta T_{\mathrm{S}}(t) = {} & \Delta T_{\mathrm{Sav}}[1 - \exp(-\lambda_1 t)] + \Delta T_{\omega} f_{\mathrm{S}}(\omega)\sin(\phi_0 + \varphi_{\mathrm{STr}})\exp(-\lambda_1 t) \\ & + \Delta T_{\omega} f_{\mathrm{S}}(\omega)\sin(\omega t + \phi_0 + \varphi_{\mathrm{S}})\end{aligned} \tag{4}$$

where ΔT_{ω} and ΔT_{Sav} are given by

$$\Delta T_{\omega} = \frac{P_{\omega}}{C_{\mathrm{P}}\omega} \tag{5a}$$

$$\Delta T_{\mathrm{Sav}} = \frac{\Delta P_{\mathrm{av}}}{C_{\mathrm{P}}\lambda_1}\left[1 + (1 - g_{\mathrm{H}})\,\mathrm{Bi} + \mathrm{O}(\mathrm{Bi}^2) + \cdots\right] \tag{5b}$$

The initial phase, ϕ_0, has been introduced because for $\Delta P_{\mathrm{av}} = 0$ the proper choice of ϕ_0 will make the transient response vanish. With φ_{STr}

given by $\cos \varphi_{STr} = [1 + \omega^2/\lambda_1^2]^{-1/2}$ and ω in the isothermal regime, ϕ_0 will be close to $-90°$. Without the approximation, the phase shift $\varphi_S(\omega)$ and correction function $f_S(\omega)$ are

$$\cos \varphi_S = (\lambda_1 \lambda_2 - \omega^2)[(\lambda_1 \lambda_2 - \omega^2)^2 + (\lambda_1 + \lambda_2)^2 \omega^2]^{-1/2} \tag{6a}$$

$$f_S(\omega) = \frac{\beta}{g_H} \omega(\lambda_2 - \lambda_1)[(\lambda_1 \lambda_2)^2 + (\lambda_1 + \lambda_2)^2 \omega^2 + \omega^4]^{-1/2} \tag{6b}$$

Corresponding expressions for $\Delta T_H(t)$ can be easily obtained. $f_S(\omega)$ takes into account the effects of radiative heat loss and the finite thermal conductivity. β is given by the components of the eigenvectors of the coefficient matrix. For $Bi \leqslant 0.01$, $\beta \approx g_H$, Eqs. (6a) and (6b) reduce to the expressions given by Sullivan and Seidel [2], and

$$\lambda_1^{-1} \approx \tau_1 = \frac{C_P}{4A\sigma\varepsilon T_o^3} \tag{7a}$$

$$\lambda_2^{-1} \approx \tau_2 = \frac{C_P g_H (1 - g_H)}{4\pi(R - \gamma\delta)\kappa} \tag{7b}$$

with an accuracy better than 10^{-2}. τ_1 and τ_2 represent the external and internal relaxation times, respectively. It should be mentioned that τ_2 agrees to better than 10% with the decay constant of the first spatial Fourier component of a transient temperature distribution in a spherical specimen, τ_F, given by [1, 11]

$$\tau_F = \frac{3C_P}{4\pi^3 R\kappa} \tag{8}$$

Regarding quantitative modulation calorimetry, the following conclusions from the simple model can be drawn. (a) For $Bi \leqslant 0.01$, there can always be found a modulation frequency ω such that $\tau_1 \ll 1/\omega \ll \tau_2$ and $1 - f_S(\omega) \leqslant 0.03$, corresponding to isothermal modulation conditions. In this case, the time scale of modulation is much slower than the decay time of internal temperature gradients and much faster than the time constant of radiative relaxation to a new equilibrium temperature. $f_S(\omega)$ can be calculated with a high accuracy and applied to a measured amplitude of temperature modulation reducing the systematic error in c_p determination originating from temperature nonuniformity below 1%. (b) $Bi \leqslant 0.01$ can be verified experimentally by (i) a purely exponential behavior of the transient temperature response and identical τ_1 at the polar and equatorial positions, (ii) from $\lambda_2 \gg \lambda_1$, as evaluated from measurement of $\varphi_S(\omega)$, and (iii) from comparison of ΔT_{Sav} and ΔT_{Hav}, which does, however, require

temperature measurement with a precision $\Delta T/T \leqslant 10^{-4}$. (c) The phase shift is a very sensitive indicator of isothermal modulation conditions, with $|\varphi_S(\omega)| < 90°$ and $|\varphi_S(\omega)| > 90°$ indicating dissipative and conductive effects, respectively. However, $\varphi_S(\omega) = -90°$ is not a sufficient condition for isothermal modulation. (d) For $\mathrm{Bi} \leqslant 0.01$ the thermal relaxation times can be obtained with a high accuracy from the transient temperature response and $\varphi_S(\omega)$. (e) For $\mathrm{Bi} > 0.01$ precise determination of $f_S(\omega)$ requires measurement of $\varphi_S(\omega)$ and $\varphi_H(\omega)$ and knowledge of g_H. (f) For poor thermal conductors, i.e., high-resistivity specimens, ac calorimetry is best performed with temperature measurement in the equatorial plane. In this case, a frequency range with $f_H(\omega) - 1 < 0.03$ can be identified. The latter is due to the fact that the lower thermal conductivity is offset by a larger directly heated volume fraction with $g_H \geqslant 0.80$.

Within the model outlined above, dissipation may also include heating power consumption by the latent heat of a phase transformation in the temperature range $T_o \pm \Delta T_\omega$. This will result in a phase shift $|\varphi_S(\omega)| < 90°$ for an ω chosen such that in the pure phase isothermal modulation conditions prevail, i.e., $\varphi_S = -90°$. In the language [12] of modulated differential thermal analysis, $|\varphi_S(\omega)| < 90°$ corresponds to a positive imaginary part of the heat capacity, $\mathrm{Im}\{c_P\} > 0$, while thermal conductivity effects correspond to $\mathrm{Im}\{c_P\} < 0$. In this terminology it can be readily visualized that the effects of dissipation and finite thermal conductivity may combine to result in $\mathrm{Im}\{c_P\} = 0$ corresponding to $\varphi_S = -90°$ without $f_S(\omega) \approx 1$.

2.3. Modulation Modes

In the metastable regime of the undercooled melt, the time required to perform a c_P measurement becomes a critical issue. The increase in average temperature as well as the initial transient require measurement times $t_{meas} > 3\tau_1$ until the stationary modulation dominates, allowing precise determination of ΔT_ω. With $\tau_1 \approx 60$ s at intermediate undercooling of the bulk metallic glass-forming alloys, t_{meas} can interfere with the onset of recalescence. To reduce t_{meas} a special modulation mode can be applied avoiding the increase in average temperature as well as the initial transient. In the amplitude mode the heater current is modulated according to $I_H(t) = I_{Ho} + I_\omega \sin(\omega t)$, while in the power mode the control voltage of the heater oscillating circuit is adjusted such that $I_H(t) = [I_{Ho}^2 + I_\omega^2 \sin(\omega t + \phi_0)]^{1/2}$, resulting in

$$\Delta P(t) = G_H[\tfrac{1}{2} I_\omega^2 + 2 I_{Ho} I_\omega \sin(\omega t) - \tfrac{1}{2} I_\omega^2 \cos(2\omega t)] \tag{9a}$$

$$\Delta P(t) = G_H I_\omega^2 \sin(\omega t + \phi_0) \tag{9b}$$

for amplitude and power modulation, respectively. G_H is the coupling coefficient between the heater field and the specimen. For power modulation the increase in average temperature is absent. Adjustment of the initial phase ϕ_0 allows the transient part of $T_S(t)$ to vanish. Depending on the specimen size, this will allow $t_{meas} < 60$ s.

3. EXPERIMENTS

3.1. Modulation Calorimetry

Experiments were performed with Zr-based metallic glass-forming alloys. Specimens with a radius of 4 mm contained in an open cage holder were positioned in the center of a quadrupole positioning field and heated by an rf dipole field. Figure 1 shows a typical ac calorimetry run in the undercooled melt in the power modulation mode. The experiment was performed with the alloy $Zr_{65}Al_{7.5}Cu_{17.5}Ni_{10}$ with liquidus temperature $T_l = 1135$ K. The specimen was cooled from a high temperature by reducing the heater power to a minimum value for a predetermined time interval and then switching the heater generator to the temperature where the measurement is to be performed. The initial phase was chosen as $\phi_0 = -90°$ to make the transient part of the temperature response vanish,

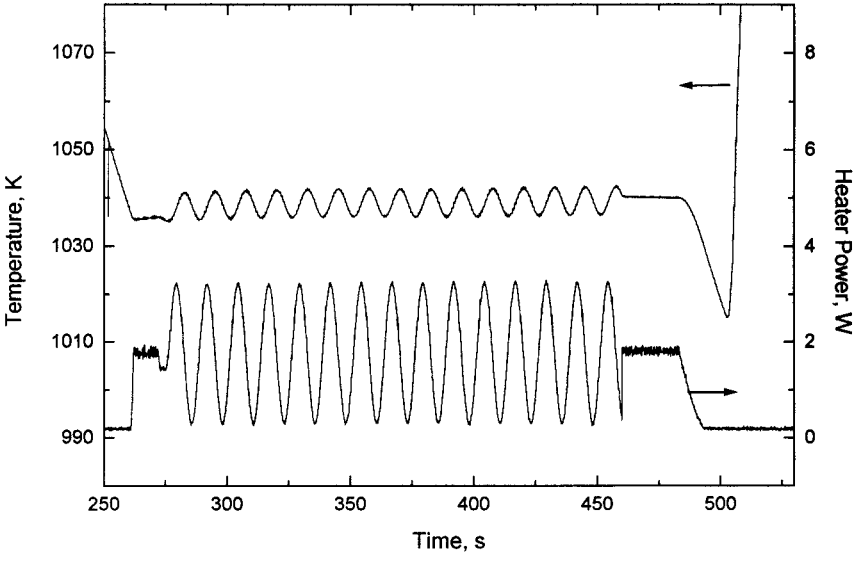

Fig. 1. Modulation calorimetry in the undercooled liquid of a $Zr_{65}Al_{7.5}Cu_{17.5}Ni_{10}$ alloy: power mode. Left ordinate, temperature; right ordinate, power.

resulting in a stationary modulation response at the onset of modulation. The rapid increase in temperature at $t = 500$ s indicates the onset of recalescence. The isothermal modulation regime was determined in ground based experiments with solid specimens to be in the range of $0.06\ \text{Hz} \leqslant \omega \leqslant 0.14\ \text{Hz}$.

3.2. Specific Heat Capacity and External Relaxation Time

For c_p determination, ΔT_ω is evaluated from the Fourier transform of the temperature signal resulting in a precision of ΔT_ω determination of better than 3%. ΔP_ω is evaluated according to the algorithm developed by Lohöfer and Egry [4]. Calibration of rf heating power input for evaluation of the specific heat from ac calorimetry has been described in detail elsewhere [6, 13]. Modulation experiments with ω in the isothermal regime are performed in the crystalline phase with well-known C_P, allowing evaluation of G_H from Eqs. (9a) or (9b) and (4). G_H depends on geometry factors, the specimen resitivity, and the radius [14, 15]. Scaling to the temperature and phase of interest is performed by inductive resistivity measurement [4] and by the optical measurement of the thermal expansion [9].

For $\text{Bi} \leqslant 0.01$, the external relaxation time can be obtained from the temperature response to a step function change in average heating power input, i.e., $\Delta P(t) = \Delta P_{av}\theta(t)$. The response reduces to the first term in Eq. (4), allowing evaluation of λ_1 with an accuracy of better than 1% from a logarithmic plot of the change in average temperature versus time. ΔP_{av} must be chosen such that $\Delta T_{Sav}/T_0 \ll 1$, with T_0 the average temperature corresponding to P_0. It has been demonstrated [5, 16] that over a large range in temperature the transient response is very well represented by a single exponential. Combined with heat capacity measurement by ac calorimetry, the total hemispherical emissivity $\varepsilon(T)$ can then be evaluated from Eq. (7a). Figure 2 shows $\varepsilon(T)$ in the liquid phase of the alloy $Zr_{60}Al_{10}Cu_{18}Ni_9Co_3$ with $T_l = 1128$ K.

$\varepsilon(T)$ exhibits a pronounced maximum at $T_m = 1175$ K. While a detailed discussion of this finding is not within the scope of this article, a few comments shall be made. First, taking the measured resistivity, the decrease in $\varepsilon(T)$ for $T < T_m$ is not in agreement with the free electron model. Second, segregation of a surface oxide layer will result in an increase in $\varepsilon(T)$. We suggest that surface segregation of low-emissivity alloy components causes the effect. This possibility is supported by the large difference in the surface tension of the pure components with $\sigma(\text{Al}) \approx 900\ \text{mN} \cdot \text{m}^{-1}$, $\sigma(\text{Cu}) \approx 1300\ \text{mN} \cdot \text{m}^{-1}$, and $\sigma(\text{Zr}) \approx 1500\ \text{mN} \cdot \text{m}^{-1}$ [17], as well as by the observation of a positive slope in the surface tension as

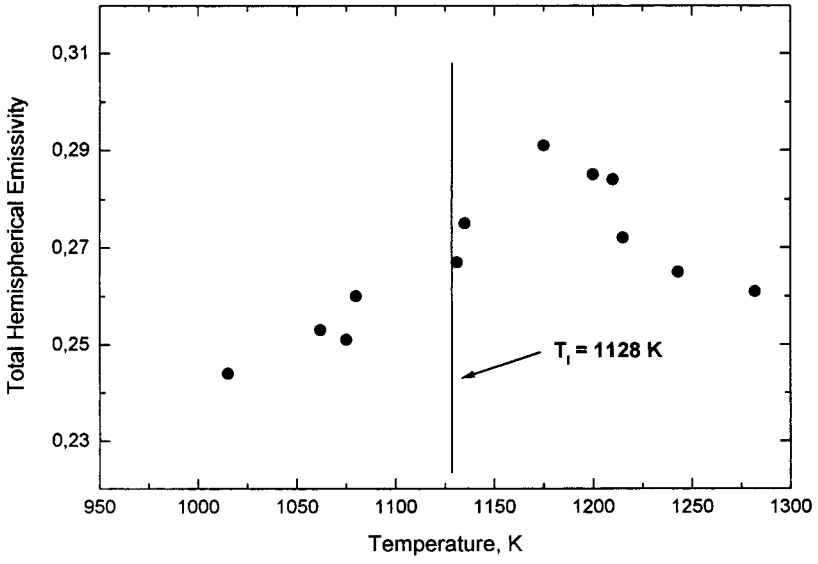

Fig. 2. Total hemispherical emissivity $\varepsilon(T)$ in the stable and undercooled liquid of $Zr_{60}Al_{10}Cu_{18}Ni_9Co_3$, with the liquidus temperature $T_l = 1132$ K indicated by the horizontal line.

a function of temperature of the alloy $Zr_{57}Cu_{15.4}Ni_{12.6}Al_{10}Nb_5$ in the same series of experiments [18]. It is conceivable that with ground-based levitation this effect may not be discerned due to the strong electromagnetic stirring or Marangoni convection in the case of laser heating of electrostatically levitated specimens. This observation is relevant for considerations of the critical cooling rate and, thus, the glass-forming ability in this type of alloy.

3.3. Internal Relaxation Time

The internal relaxation time is evaluated from measurement of $\varphi_S(\omega)$ with ω tuned to a value above the isothermal regime. Ideally this measurement should be performed for several values of ω. Due to limited sample stability in the space experiment, only $\omega = 0.16$ Hz was applied. With τ_1 obtained from the transient response, τ_2 was evaluated from $\varphi_S(\omega)$ and Eq. (6a). Table I shows $\varphi_S(\omega)$, τ_2, and κ for the alloy $Zr_{65}Al_{7.5}Cu_{17.5}Ni_{10}$. κ was evaluated from Eq. (10). Comparing with $\varphi_S(0.08\ \text{Hz}) = (90.4 \pm 0.5)^\circ$, the effect of the finite thermal conductivity is clearly discerned, while regarding $f_S(\omega)$ the effect is small, i.e., $1 - f_S(0.16\ \text{Hz}) < 0.03$. However, for $\text{Bi} \leqslant 0.01$, the evaluation of τ_1 and τ_2 from $\Delta T(t)$ and $\varphi_S(\omega)$ is very

Table I. Phase Shift φ_S Between Heater Current and Temperature Response, Internal Relaxation Time τ_2, and Thermal Conductivity κ

T_0 (K)[a]	ω (Hz)	φ_S (deg)	τ_2 (s)	κ ($W \cdot cm^{-1} \cdot K^{-1}$)
1033^x	0.16	99.8	0.19	0.21
1024^l	0.16	100.0	0.20	0.38
1196^l	0.16	97.2	0.17	0.34

[a] Superscripts x and l refer to the solid and liquid phases, respectively.

accurate, and the determination of the physical transport properties ε and κ depends on the particular transport model. Radiative heat loss of a sphere at uniform temperature as represented in Eq. (7a) is well justified for ε determination. However, Eqs. (7b) and (8) represent an approximation to the actual polar transport mode. The systematic error in κ is estimated as $\leqslant 10\%$. Higher accuracy requires detailed modeling of the heat flow. A systematic error of $\leqslant 10\%$ does, however, compare very well with results from the laser flash method. The accuracy of the κ evaluation by Eq. (8) is supported by comparing $\kappa(1033\ K) = 0.21\ W \cdot cm^{-1} \cdot K^{-1}$ obtained from the modulation measurements at the calibration temperature in the solid phase with $\kappa(1033\ K) = 0.23\ W \cdot cm^{-1} \cdot K^{-1}$, obtained from application of the Wiedemann–Franz law with an independently measured resistivity of $\rho(1033\ K) = 115\ \mu\Omega \cdot cm$.

The thermal conductivity in the liquid phase represents an effective value including a contribution from electromagnetic forced convection. This effect can be clearly discerned. Scaling τ_2 according to $\tau_2 \propto c_P \rho / T$ into the liquid phase would result in $\tau_2(1156\ K) = 0.36$ s, compared to a measured value $\tau_2 = 0.17$ s. Thus, forced convection by the heater and positioner fields contributes about half to the relaxation time of internal temperature gradients. With the viscosity obtained from, e.g., oscillating drop experiments [19], all necessary thermophysical properties can be measured in TEMPUS to allow modeling of the temperature and fluid flow field with the thermal conductivity of the liquid as a free parameter. Thus, ac calorimetry with ω variation, combined with numerical modeling, provides an approach for determination of the thermal conductivity in the liquid phase.

3.4. Modulation Calorimetry in the Two-Phase Region

Modulation calorimetry in the two-phase region can be applied to investigate the dynamics of the melting process [20], the solid fraction,

and potentially the thermal conductivity. These properties are of considerable importance in the modeling of industrial casting and solidification processes [21]. As an example, Fig. 3 shows ac calorimetry in the two-phase region of a $Zr_{64}Ni_{36}$ specimen with a slightly off-eutectic composition resulting in a melting interval of ≈ 15 K. A modulation frequency of $\omega = 0.10$ Hz was applied, corresponding to isothermal modulation in the pure phases. A continuous increase in average temperature was subtracted from the ac temperature signal. The response is characterized by an increase in ΔT_ω and a continuous change in φ_S from $\varphi_S = -78°$ to $\varphi_S \to -90°$ as a function of modulation duration, i.e., the underlying temperature increase. The reduction in ΔT_ω, compared to a measurement performed at $T_l + 50$ K and $|\varphi_S| < 90°$, is the result of a loss process, with part of P_ω consumed for melting a crystalline fraction. In a first approach, quantification can be obtained by considering that the enthalpy consumed per half-cycle for melting, $\frac{1}{2}\omega P_{melt} = \Delta H_f f_x m$, can be obtained from $P_{melt} = P_\omega - \Delta T_\omega (1 - f_x)\, mc_p^l \omega$ with m and f_x the mass and solid fractions, respectively. P_ω corresponds to the amplitude of power modulation, i.e., $P_\omega = 2G_H I_{Ho} I_\omega$ for amplitude modulation, and the last term to the power

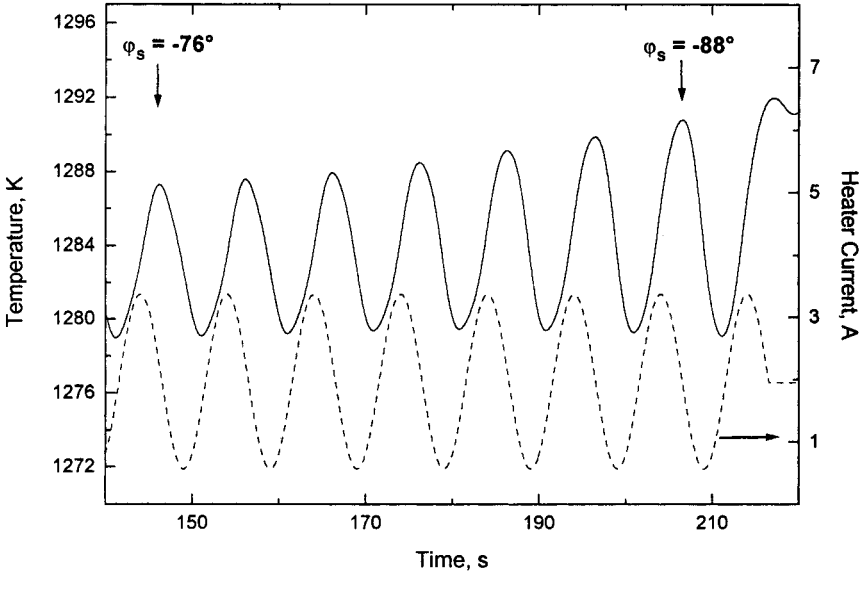

Fig. 3. Ac calorimetry in the two-phase region; $Zr_{64}Ni_{36}$ with a slightly off-eutectic composition. Left ordinate, temperature (solid line); right ordinate, power input (dashed line). φ_S: phase shift between heater power and temperature response at the temperature maxima indicated by arrows.

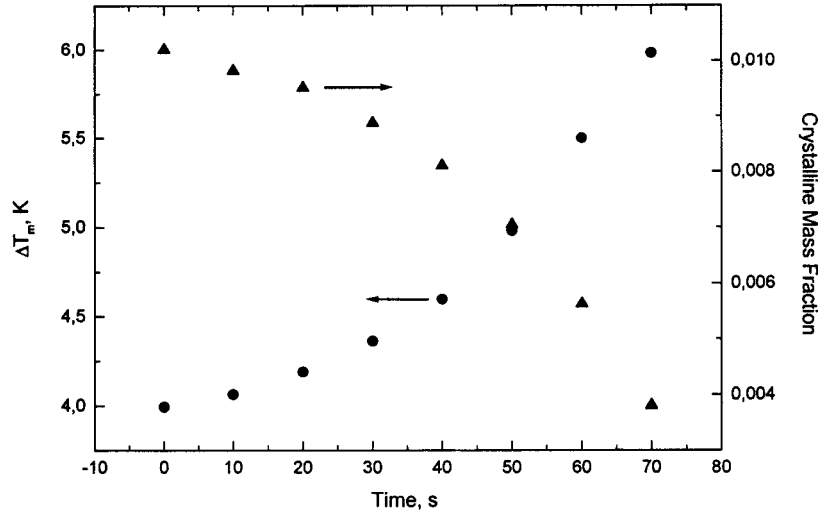

Fig. 4. Two-phase region; $Zr_{64}Ni_{36}$. Left ordinate, amplitude of temperature modulation (circles); right ordinate, solid fraction (triangles).

consumed for heating the liquid, Eq. (5a). This approach was used to obtain the solid fraction as a function of modulation duration shown in Fig. 4, demonstrating the high sensitivity of ac calorimetry to the presence of a small crystalline fraction.

4. SUMMARY

Noncontact ac calorimetry based on electromagnetic heating and positioning has evolved into a quantitative measurement method allowing precise determination of the specific heat, enthalpy of fusion, and thermal relaxation times, from which the corresponding transport properties can be evaluated. In addition, the applicability of noncontact ac calorimetry in the two-phase region was demonstrated. This application shall be further investigated regarding properties such as interfacial mobility, solid fraction, and thermal conductivity in the two-phase region. Experiments were performed with the containerless processing device TEMPUS in two μg experiments. While in the preceding experiments this technique was applied to the investigation of the thermodynamic functions of metallic glass-forming alloys, in the future it is planned to apply these techniques to the measurement of thermophysical properties of reactive metallic alloys of industrial relevance.

ACKNOWLEDGMENTS

We gratefully acknowledge support by Dr. G. Lohöfer of the German Space Establishment (DLR) in the resistivity measurement and by Dr. B. Damaschke (University of Göttingen) in the analysis of specimen shape. Funding by the German space agency DLR (DARA Grant 50 WM 94-31-4) is gratefully acknowledged. H.J.F. acknowledges support from the European Space Agency Topical Team on properties of liquids as well as support from the Deutsche Forschungsgemeinschaft (G. W. Leibniz Programm).

REFERENCES

1. H.-J. Fecht and W. L. Johnson, *Rev. Sci. Instr.* **62**:1299 (1991).
2. P. F. Sullivan and G. Seidel, *Phys.Rev.* **173**:679 (1968).
3. Y. A. Kraftmakher, *Compendium of Thermophysical Property Measurement Methods*, K. D. Maglic, A. Cezairliyan, and V. E. Peletsky, eds. (Plenum Press, New York, 1992), Vol. 1, pp. 591–641, Vol. 2, pp. 409–434.
4. G. Lohöfer and I. Egry, *Solidification 99*, W. H. Hofmeister, J. R. Rogers, N. W. Sing, S. P. March, and P. W. Vorhees, eds. (TMS, Warrandale, PA, 1999), pp. 65–74.
5. R. K. Wunderlich and H.-J. Fecht, *Int. J. Thermophys.* **17**:1203 (1996).
6. R. K. Wunderlich, D. S. Lee, W. L. Johnson, and H.-J. Fecht, *Phys. Rev. B* **55**:26 (1997).
7. I. Egry, *J. Jpn. Soc. Micrograv. Appl.* **15**:215 (1998).
8. W. H. Hofmeister, R. J. Bayuzick, and S. Krishnan, *Space Processing of Materials*, N. Ramachandran, ed., *Proc. SPIE*, Vol. 2809 (1996), pp. 288–302.
9. B. Damaschke, D. Oelgeschläger, J. Ehrich, E. Dietzsch, and K. Samwer, *Rev. Sci. Instr.* **69**:2110 (1998).
10. B. Q. Li, *Int. J. Eng. Sci.* **31**:201 (1993).
11. H. S. Carslaw and J. C. Jaeger, *Conduction of Heat in Solids* (Oxford University Press, Oxford, 1959), pp. 230–238.
12. J. E. K. Schawe and G. W. H. Höhne, *J. Therm. Anal.* **46**:893 (1996).
13. R. K. Wunderlich, Ch. Ettl, A. Sagel, H. J. Fecht, D. S. Lee, S. C. Glade, and W. L. Johnson, *Solidification 99*, W. H. Hofmeister, J. R. Rogers, N. W. Sing, S. P. March, and P. W. Vorhees, eds. (TMS, Warrandale, PA, 1999), pp. 53–64.
14. E. Fromm and H. Jehn, *Br. J. Appl. Phys.* **16**:653 (1965).
15. G. Lohöfer, *SIAM J. Appl. Math.* **49**:567 (1989).
16. R. K. Wunderlich, H.-J. Fecht, and R. Willnecker, *Appl. Phys. Lett.* **62**:3113 (1993).
17. T. Iida and R. I. L. Guthrie, *The Physical Properties of Liquid Metals* (Clarendon Press, Oxford, 1993).
18. M. Roesner-Kuhn, *Microgravity Science Laboratory (MSL-1) FinalReport*, NASA/CP—1998-208868 (1998), pp. 232.
19. S. Sauerland, K. Eckler, and I. Egry, *J. Mater. Sci. Lett.* **11**:330 (1992).
20. K. A. Q. O'Reilly and B. Cantor, *Proc. R. Soc. Lond. A* **452**:2141 (1996).
21. H.-J. Fecht, Proposal to the European Space Agency (1999).